Journal of Nuclear Materials 498 (2018) 254–258

Contents lists available at ScienceDirect

Journal of Nuclear Materials

journal homepage: www.elsevier.com/locate/jnucmat

Short communication on Kinetics of grain growth and particle pinning in U-10 wt.% Mo

William E. Frazier*, Shenyang Hu, Nicole Overman, Curt Lavender, Vineet V. Joshi

Pacific Northwest National Laboratory, 902 Battelle Boulevard, Richland, WA 99354-1793, USA

ARTICLE INFO

Article history:
Received 7 August 2017
Received in revised form
21 September 2017
Accepted 16 October 2017
Available online 20 October 2017

ABSTRACT

The alloy U-10 wt% Mo was annealed at temperatures ranging from 700 °C to 900 °C for periods lasting up to 24 h. Annealed microstructures were examined using Electron Backscattered Diffraction (EBSD) to obtain average grain sizes and grain size distributions. From the temporal evolution of the average grain size, the activation energy of grain growth was determined to be 172.4 ± 0.961 kJ/mol. Grain growth over the annealing period stagnated after a period of 1–4 h. This stagnation is apparently caused by the pinning effect of second-phase particles in the materials. Back-scattered electron imaging (BSE) was used to confirm that these particles do not appreciably coarsen or dissolve during annealing at the aforementioned temperatures.

UMo alloys are currently being explored as potential replacements for highly enriched uranium (HEU) fuels used in advanced research nuclear reactors [1,2]. The addition of Mo to the uranium retains the gamma phase and the γ-U phase has isotropic thermomechanical properties, high U-density, and excellent irradiation resistance [3,4]. U-10Mo is of particular interest because the composition brings additional stability to the γ-U phase at reactor operating temperatures without undergoing any phase transformation [5]. Further, U-10Mo has greater ductility and fracture toughness than U-12Mo and greater stress corrosion cracking resistance than U-7Mo [6].

While homogenization and the thermomechanical processing of the alloy has been explored [4,5], the grain growth behavior of the homogenized and thermomechanically processed alloy has not been investigated. For example, Burkes reports that a small amount of grain coarsening occurs when annealing U-10Mo at 650–657 °C, but does not quantify these observations [6]. Understanding the grain growth kinetics is of particular importance as it is believed that UMo microstructure will significantly affect the phase transformation kinetics and also the fuel material response under irradiation. Hu et al. predicts through modeling that swelling kinetics with respect to fission density in γ-UMo depend upon grain size and grain aspect ratio, occurring the fastest as grain size decreases and aspect ratio increases [7], although experimental verification of this is still forthcoming. Previous work has established the presence of two secondary phases in U-10Mo: Uranium Carbide (UC) and a Mo-Si-U-C quaternary compound [8]. The grain growth behavior of polycrystalline materials in the presence of second phase particles has been the subject of experimentation on a wide variety of materials systems for decades [9–16]. Therefore, one can presume UMo will perform optimally under irradiation when its grains are large and equiaxed.

In order to define U-10Mo processing parameters for achieving desired microstructure and fuel performance, this work examined the grain growth behavior of U-10Mo between the temperatures of 700 °C and 900 °C. This is above the eutectoid temperature of U-Mo [17–19]. The activation energy of U-10Mo grain growth at rolling temperatures was determined with the temporal evolution of grain size. The pinning effect of second phase particles on grain growth was analyzed.

A U-10.4 wt% Mo alloy was used to prepare rolled foils. Hot- and cold-rolling was performed on a Stanat model TA-215, two-high mill that was later transformed to four-high mill for cold-rolling operations to attain the desired foil thickness. In the two-high configuration, the top and bottom rolls were 4 inches in diameter and roughly 8 inches wide; whereas in the four-high mill configuration the 7/8-inch rolls were backed with 4-inch rolls. The rolling experiments were performed without lubrication. To roll the depleted U-10Mo samples, they were wrapped in zirconium foils roughly 0.001-inch (0.025 mm) thick. The mill was operated at 25 revolutions per minute (rpm) and had a maximum load

* Corresponding author.
E-mail address: william.frazier@pnnl.gov (W.E. Frazier).

https://doi.org/10.1016/j.jnucmat.2017.10.041
0022-3115/

separation force of 100,000 lb. The samples were hot rolled from 0.2 inch (5.08 mm) to 0.04 inch (1.02 mm), with 15% reductions per pass, and were pre-heated in air at 700 °C for 20–30 min in a Thermcraft Model 1134 tube furnace before each pass. The samples were immediately rolled (within 5 s) to minimize heat loss during the hot-rolling procedure. Upon attaining the desired thickness of 0.04 inch (1.02 mm), the samples were then stress relief annealed at 700 °C for 1 h in an MTI model VBF-1200X-H8 furnace in a continuously flowing argon atmosphere and later etched to remove any surface oxides that may have formed during the rolling and annealing operations. The samples were subsequently cold rolled in the 4-high mill configuration with ~10% reductions per pass to attain a final thickness of 0.0085 inch (0.203 mm). Cold-rolled foils were later heat treated inside an Ar-atmosphere furnace at 700 °C for 1 h. Later the recrystallized samples were annealed at 700 °C, 800 °C, and 900 °C for periods of 1 h–24 h.

After the heat treatment, individual samples were mounted in epoxy, ground, and polished to a 0.05 μm finish using a standard metallographic procedure [20]. To characterize the extent of phase transformation in the studied alloy, optical microscopy and scanning electron microscopy imaging were employed. Optical images were captured using polarized light, which can readily resolve the grain structure in the UMo alloy in its polished condition. A scanning electron microscope (SEM; JEOL JSM-7600F) equipped with an energy-dispersive x-ray spectroscopy (EDS) detector (Oxford Instruments X-Max 80) was used. EDS software (INCA Microanalysis Suite Version 4.15) was used to study phase composition. Electron back-scattered diffraction (EBSD) analysis was also performed for grain size estimation. X-ray diffraction (XRD) analysis, conducted for phase identification, involved the use of a Rigaku Ultima IV x-ray diffractometer equipped with a monochromated Cu K-α x-ray source and a linear position-sensitive silicon strip detector. In general, diffraction data were collected between 25° and 120° 2θ in 0.001° increments at a scan rate of 0.5°/min. Micrographs of the second-phase particles were obtained using BSE-SEM at a magnification of 500×.

Grain growth behavior is regularly described by the n-power law [21–25], which follows the form:

$$d^n - d_0^n = k_0 t e^{-Q_{Act}/RT} \quad (1)$$

For normal, curvature-driven grain growth, $n = 2$. Here, Q_{Act} is the activation energy of grain growth, k_0 is a constant, T is absolute temperature, and R is the universal gas constant. It is well known that Q_{Act} and k_0 can be obtained from fitting the observed grain growth coefficient k into an Arrhenius relationship with T. Actual behavior can deviate from this ideal case for multiple reasons, most notably the occurrence of grain boundary pinning [26–28] and solute dissolution [15,29]. For this work, we assumed $n = 2$, and that the second phases present in the alloy remain inert between 700 °C and 900 °C.

Fig. 1 shows the temporal evolution of average grain sizes for 700 °C, 800 °C, and 900 °C annealing treatments. Grain growth kinetics increases dramatically with the increase of annealing temperature. The most rapid period of grain growth occurs in the first hour of annealing, followed by a period of stagnated grain growth. At 700 °C, average grain diameter remains within the margin of error of the as-rolled and annealed material throughout the entire period.

The microstructures of U-10Mo samples annealed at different temperatures and times are shown in Figs. 2–3, alongside their grain size distributions. Visual inspection of the micrographs confirms the general trends shown in Fig. 1.

As annealing continues and temperature increases, the grain size distribution becomes increasingly wide, and the tail of the distribution becomes longer. This effect is small for the 700 °C anneal and considerably more pronounced for the 900 °C anneal. The widening of the grain size distribution indicates that due to an inhomogeneity in the distribution of particles within the microstructure, some of the grains were able to grow to a larger extent before becoming pinned.

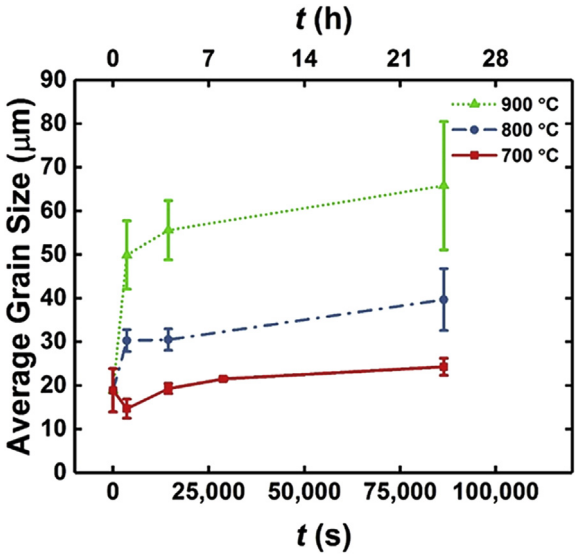

Fig. 1. The average grain diameter of U-10Mo over annealing at 700 °C, 800 °C, and 900 °C. Grain growth follows a power-law relationship throughout the 24 h period of annealing.

The activation energy of grain growth was calculated from the average grain size data in Fig. 1 from 0 to 4 h of annealing. We assumed that during this period, the grain growth is curvature driven and relatively uninhibited by particle pinning ($n = 2$). In order to obtain an estimate of the activation energy of uninhibited U-10Mo grain growth as opposed to the activation energy of the aggregate grain growth behavior, we therefore exclude the remainder of the grain growth data from the calculation. Based on this premise, we calculate an activation energy for grain growth of 172.4 kJ/mol ± 0.961 kJ/mol (Fig. 4.). We can further calculate the value of the grain growth constant k_0, as 7.66×10^{-6} m^2/s.

BSE-SEM micrographs of U-10Mo microstructure (Fig. 5a–b) show the second phase particles prominently, distinguished by their darker shades of gray. From visual inspection, these particles do not appear to have coarsened or dissolved. Further, the chemical inhomogeneity indicated by the sections of black within the particles, likely Si-rich, remains. This confirms our assumption in fitting the activation energy that the second-phase particles are inert.

The activation energy of grain growth is an important material parameter from a processing standpoint. For example, we can easily use Q_{Act} and k_0 with the n – power law to estimate the amount of annealing time required to reach a target grain size, for example. The activation energy of grain growth can also provide time scaling for grain growth simulation algorithms, such as the Potts Model or Phase Field Models.

Experimental data on the activation energy of grain growth in U-alloys is scarce. Only one effort to our knowledge exists for U-Mo alloys, in which Mei et al. used data from two unpublished efforts to estimate a grain growth activation energy of 272.3 kJ/mol in U-7Mo [30]. The reason for this discrepancy is not immediately clear. Two

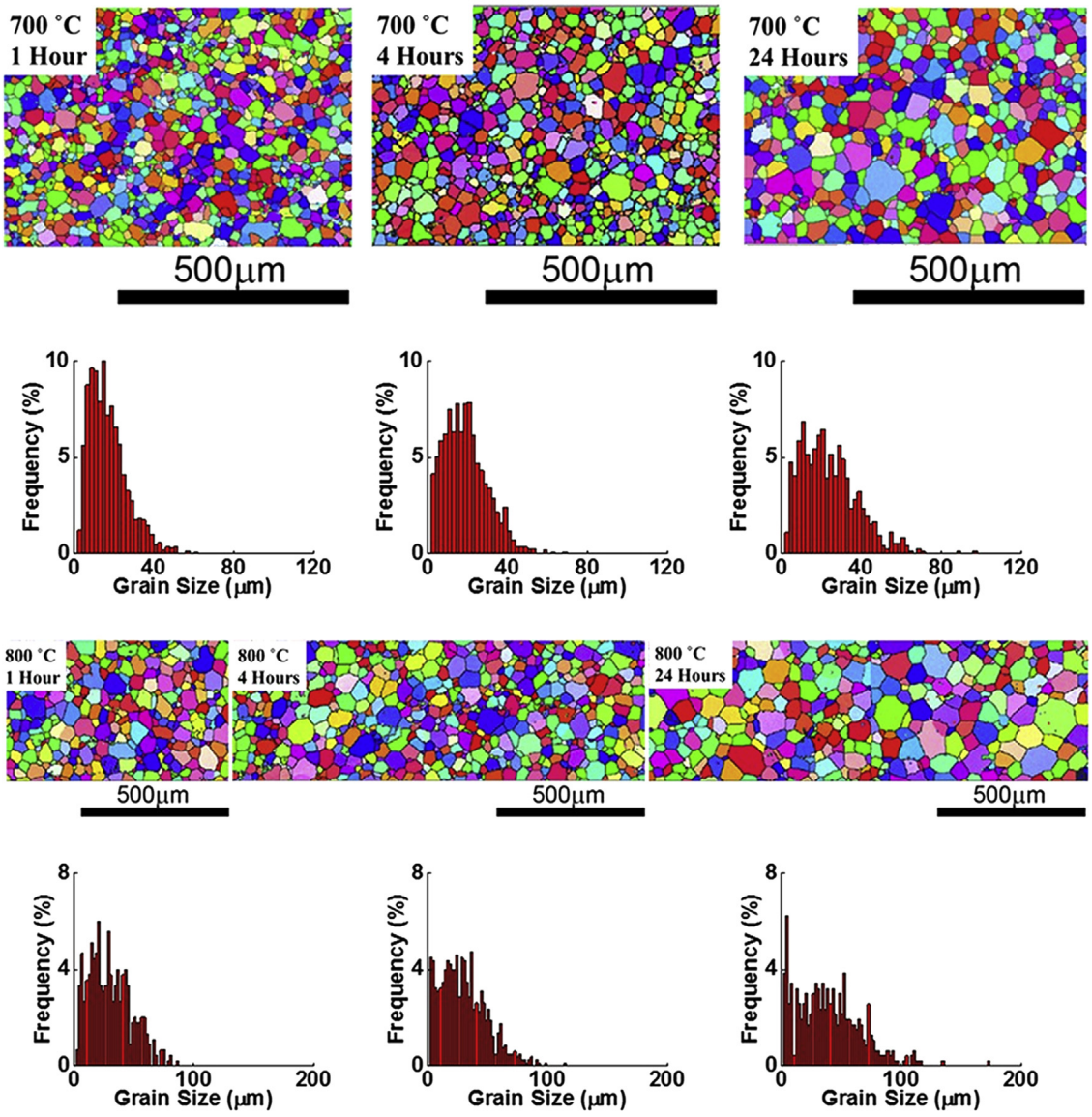

Fig. 2. EBSD micrographs of U-10Mo obtained from samples annealed at 700 °C and 800 °C, alongside the corresponding histograms of their grain size distributions.

other efforts have measured the activation energy of grain growth in U-Nb alloys, though the alloying element (Nb) and phase of Uranium (α-U) are both different from the fuel of interest [31]. Table 1 shows the activation energies of grain growth for these and several other alloy systems.

Assuming that the second phase particles occupy 2.0% of the sample surface and the average particle radius is 0.2 μm, we can estimate a maximum average grain diameter of 26.7 μm using the Zener equation [38]. Grain growth stagnates at approximately this grain size during the 700 °C anneal, but is nearly 40 μm at 800 °C and 60 μm at 900 °C. This strong temperature dependence of grain size at which grain growth stagnates indicates that the pinning effect of particles depends on the temperature. This phenomena has previously been explained by the occurrence of particle dissolution [15,29], which has the effect of increasing the Smith-Zener limit [38], but there does not appear to be any particle dissolution in our system. It is possible that some particle coarsening occurs via Ostwald Ripening [39], but this appears to occur very slowly at annealing temperature. Further, the kinetics of Ostwald Ripening are more weakly time dependent than grain growth [39,40]. Another interpretation of this behavior is that the thermal fluctuations of grain boundaries during annealing allow a sufficient number of grain boundaries to escape pinning and become mobile with increased annealing temperature. The possibility of similar behavior as a cause for abnormal grain growth was recently demonstrated in simulation by Holm [41]. This phenomenon also explains the rapid grain growth that occurs during the first hour of annealing at 800 °C and 900 °C.

In conclusion, grain growth behavior in a homogenized U-10Mo alloy was observed during anneals at 700 °C, 800 °C, and 900 °C for annealing periods of up to 24 h. From the grain growth observed, we can estimate that the activation energy for grain growth is approximately 172.4 kJ/mol ± 0.961 kJ/mol. Grain growth stagnation in U-10Mo appears to occur because two species of second-phase particles pin the grain boundaries. These particles did not appear to dissolve or coarsen appreciably over the course of the annealing period.

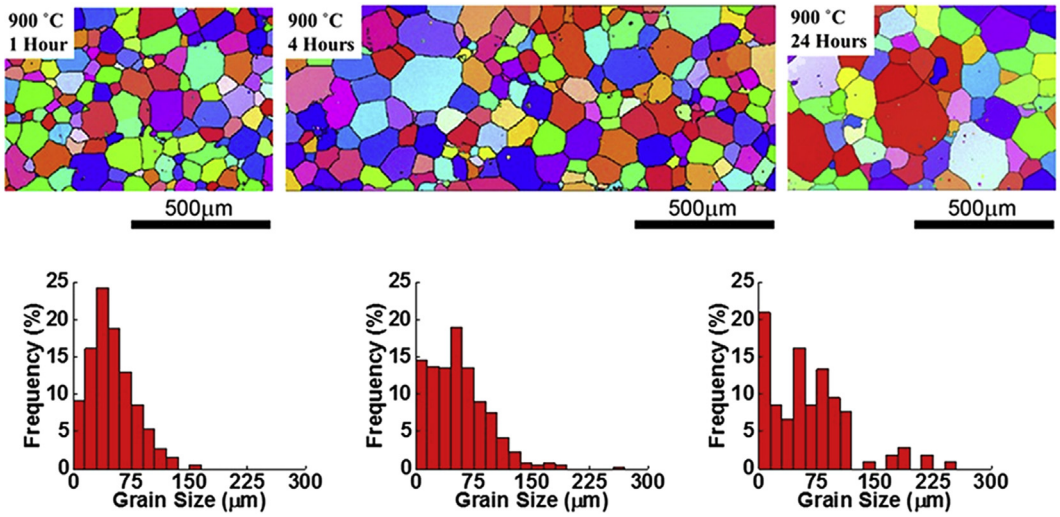

Fig. 3. EBSD micrographs of U-10Mo obtained from samples annealed at 900 °C, alongside the corresponding histograms of their grain size distributions.

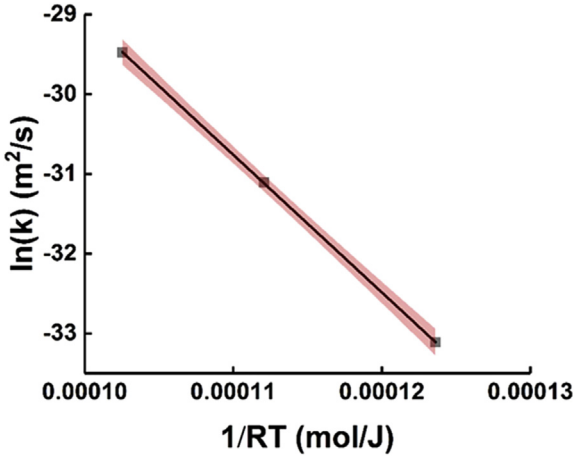

Fig. 4. The grain growth power law constant k as affected by temperature, transformed to obtain the activation energy of grain growth, Q_{Act}. We estimate that $Q_{Act} = 172.4$ kJ/mol ± 0.961 kJ/mol, with $k_0 = 7.66 \times 10^{-6}$ m^2/s. The region shown in red denotes the region of 95% confidence in our linear fit. (For interpretation of the references to colour in this figure legend, the reader is referred to the web version of this article.)

Table 1
Grain growth Activation energies for different alloy systems.

Alloy	Activation Energy (kJ/mole)
U-7Mo [30]	272.3
U-10Mo (Observed)	172.4
U-7.4Nb [32]	29.3
U-6.5Nb [33]	100.4
Cu (Ultrafine) [9]	100
Ag (Ultrafine) [9]	100
Ni-P (Austenite) [10]	182
Steels [11–16]	400–900
Iron (Pure) [35]	355
Iron (Nanocrystalline) [36]	75
Aluminum [37]	113

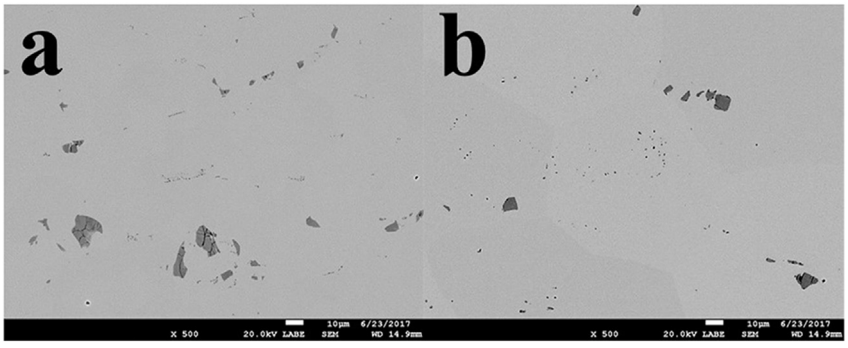

Fig. 5. BSE-SEM micrographs of the as-received U-10Mo (a) and the same material after 24 h of annealing at 900 °C (b).

Acknowledgements

The work described in this article was performed by Pacific Northwest National Laboratory, which is operated by Battelle for the United States Department of Energy under Contract DE-AC05-76RL01830. This work was performed in support of the fuel fabrication (FF) pillar for conversion of high performance research reactors from high enriched uranium to low enriched uranium. This

work supports the development and deployment of cost-efficient fuel fabrication.

References

[1] S.M. McDeavitt, A.A. Solomon, Hot isostatic pressing of U-10Zr by a coupled grain boundary diffusion and creep cavitation mechanism, J. Nuc. Mater 228 (1996).
[2] L.C. Walters, B.R. Seidel, J.H. Kittel, Nucl. Technol. 65 (1984) 202.
[3] J.-F. Jue, T.L. Trowbridge, C.R. Breckenridge, G.A. Moore, M.K. Meyer, D.D. Keiser Jr., Effects of heat treatment on U-Mo fuel foils with a zirconium diffusion barrier, J. Nuc. Mat. 460 (2015) 153–159.
[4] A.J. Clarke, K.D. Clarke, R.J. McCabe, C.T. Necker, P.A. Papin, R.D. Field, A.M. Kelly, T.J. Tucker, R.T. Forsyth, P.O. Dickerson, J.C. Foley, H. Swenson, R.M. Aikin Jr., D.E. Dombrowski, Microstructural evolution of a Uranium-10 wt.% molybdenum alloy for nuclear reactor fuels, J. Nuc. Mat. 465 (2015) 784–792.
[5] Z. Xu, V. Joshi, S. Hu, D. Paxton, C. Lavender, D. Burkes, Modeling the homogenization kinetics of as-cast U-10wt% Mo alloys, J. Nuc. Mat. 471 (2016) 154–164.
[6] D.E. Burkes, R. Prabhakaran, T. Hartmann, J.-F. Jue, F.J. Rice, Properties of DU-10wt% Mo alloys subjected to various post-rolling heat treatments, Nuc. Eng. Des. 240 (2010) 1332–1339.
[7] S. Hu, V.V. Joshi, C.A. Lavendar, N.J. Lombardo, J. Wight, B. Ye, Z.-G. Mei, L. Liang, A.M. Yacout, G. Hofman, Y. Zhang, B. Beeler, X.-M. Bai, J. Cole, B. Robin, Microstructural Level Fuel Performance Modeling of UMo Monolithic Fuel, Report Prepared for the U.S. Department of Energy, Office of NA, Under DOE Idaho Operations Office, 2016.
[8] A. Devaraj, V.V. Joshi, S. Manandhar, C.A. Lavender, L. Kovaril, S. Jana, B.W. Arey. High Resolution Characterization of UMo Alloy Microstructure. Pacific Northwest National Laboratory (2016). Report #26020 Prepared for the U.S. Department of Energy, Office of NA, Under DOE Idaho Operations Office. 2016.
[9] P.A. Manohar, M. Ferry, T. Chandra, Five decades of the Zener equation, ISIJ Int. 38 (1998) 913–924.
[10] N.P. Goss, New development in electrical strip steels characterized by fine grain structure approaching properties of single crystal, Am. Soc. Metals Trans. 23 (1935) 511–531.
[11] R.D. Doherty, D.A. Hughes, F.J. Humphreys, J.J. Jonas, D. Juul Jensen, M.E. Kassner, W.E. King, T.R. McNelley, H.J. McQueen, A.D. Rollett, Current issues in recrystallization: a review, Mater. Sci. Eng. A 238 (1997) 219–274.
[12] Z. Jin, D. Yu, X. Wu, K. Yin, K. Yan, Drag effects of solute and second phase distributions on the grain growth kinetics of pre-extruded Mg-6Zn alloy, J. Mater. Sci. Technol. 32 (2016) 1260–1266.
[13] D. Dong, F. Chen, Z. Cui, Modeling of austenite grain growth during austenitization in a low alloy steel, J. Mater. Eng. Perform. 25 (2016) 152–164.
[14] I.S. Wani, G. Dan Sathiarj, M.Z. Ahmed, S.R. Reddy, P.P. Bhattacharjee, Evolution of microstructure and texture during thermo-mechanical processing of a two phase $Al_{0.5}$CoCrFeMnNi high entropy alloy, Mater. Charact. 118 (2016) 417–424.
[15] M. Liu, W.-J. Zheng, J.-Z. Xiang, Z.-G. Song, E.-X. Pu, H. Feng, Grain growth behavior of inconel 625 superalloy, J. Iron Steel Res. Int. 23 (2016) 1111–1118.
[16] V.B. Oliveira, H.R.Z. Sandim, D. Raabe, Abnormal grain growth in Eurofer-97 steel in the ferrite phase field, J. Nuc. Mater 485 (2017) 23–38.
[17] F. Rough, A. Bauer, Constitution of Uranium and Thorium Alloys, BMI-1300, Battelle Memorial Institute, 1958, p. 41.
[18] T. Massalski, H. Okamoto, P. Subramanian, L. Kacprzak, Binary Alloy Phase Diagram, second ed., ASM International, Materials Park, OH, 1990.
[19] M.A. Steiner, C.A. Calhoun, R.W. Klein, K. An, E. Garlea, S.R. Agnew, α-phase transformation Kinetics of U – 8 wt% Mo established by in situ neutron diffraction, J. Nuc. Mater 477 (2016) 149–156.
[20] F.J. Humphreys, Quantitative metallography by electron backscattered diffraction, J. Microsc. 195 (1999) 170–185.
[21] A.D. Rollett, G. Gottstein, L. Shvindlerman, D. Molodov, Grain boundary mobility: a brief review, Z. Met. 95 (2004) 4.
[22] C.V. Thompson, Grain growth in thin films, Annu. Rev. Mater. Sci. 20 (1990) 245.
[23] R.E. Reed-Hill, R. Abbaschian, Physical Metallurgy Principles, third ed., PWS Publishing Company, Boston, 1994.
[24] P.A. Beck, J.C. Kremer, L.J. Demer, et al., Grain growth in high-purity aluminum and in an aluminum-magnesium alloy, Trans. AIME 175 (1948) 372.
[25] T. Schlenker, M.L. Valero, H.W. Schock, J.H. Werner, Grain growth studies of thin Cu(In, Ga)Se_2 films, J. Cryst. Growth 264 (2004) 178–183.
[26] B. Yuksel, O.T. Ozkan, Grain growth kinetics for B_2O_3-doped ZnO ceramics, Mater. Sci. Pol. 33 (2015) 220–229.
[27] K. Wang, M.Q. Li, C. Li, δ and austenite phases evolution and model in solution treatment of superalloy GH4169, Mater. Sci. Technol. 29 (2013) 346–350.
[28] A.A. Fasching, G.R. Edwards, S.A. David, Grain growth kinetics of an iron aluminide alloy, Scr. Metall. Mater 30 (1994) 1003–1008.
[29] A. Gangulee, F.M. D'Heurle, Anomalous large grains in alloyed aluminum thin films. 1. Secondary grain-growth in aluminum-copper films, Thin Solid Films 12 (1972) 399.
[30] Z.-G. Mei, L. Liang, Y.S. Kim, T. Wiencek, E. O'Hare, A.M. Yacout, G. Hofman, M. Anitescu, Grain growth in U-7Mo alloy: a combined first-principles and phase Field study, J. Nuc. Mater 473 (2016) 300–308.
[31] D.W. Brown, M.A.M. Bourke, A.J. Clarke, R.D. Field, R.E. Hackenberg, W.L. Hults, D.J. Thoma, The effect of low temperature aging on the microstructure and deformation of uranium- 6 wt% niobium: an in-situ neutron diffraction study, J. Nuc. Mater 481 (2016) 164–175.
[32] R.J. Jackson, R.L. Thomas, Grain Growth and the Recrystallized Grain Size for the Uranium-7.4 Weight Percent Niobium Alloy. Report to the U.S. Department of Energy. Compiled and Distributed by the NTIS, U.S. Department of Commerce, 1988. Report Number RFP-4156.
[33] Z. Xinjian, W. Xiaolin, L. Chao, Z. Nanqiang, Experimental study on recrystallized grain growth of cold-spun U-6.5Nb alloy, Rare Metal Mater. Eng. 39 (2010) 1815–1819.
[35] G. Riotino, C. Antonione, L. Battezzati, F. Marino, M.C. Tabasso, Kinetics of abnormal grain growth in pure iron, J. Mater. Sci. 14 (1979) 86–90.
[36] H. Natter, M. Schmelzer, M.-S. Löffler, C.E. Krill, A. Fitch, R. Hempelmann, Grain-growth kinetics of nanocrystallne iron studied in situ by synchrotron real-time X-ray diffraction, J. Phys. Chem. B 104 (2000) 2467–2476.
[37] W.B. Nowak, Discussion of grain growth in aluminum, Metall. Trans. A 7A (1976) 1503.
[38] C.S. Smith, Introduction to grains, phases, and interfaces: an interpretation of microstructure, Trans. Am. Inst. Min. Eng. 175 (1948) 15–51.
[39] I.M. Lifshitz, V.V. Slyozov, The kinetics of precipitation from supersaturated solid solutions, J. Phys. Chem. Solids 19 (1961) 35–50.
[40] T. Zhou, H.S. Zurob, R.J. O'Malley, K. Rehman, Model Fe-Al steel with exceptional resistance to high temperature coarsening. Part 1: coarsening mechanism and particle pinning effects, Metall. Mater. Trans. A 46A (2015) 178–189.
[41] E.A. Holm, T.D. Hoffman, A.D. Rollett, C.G. Roberts, Particle assisted abnormal grain growth. IOP con. Series, Mater. Sci. Eng. 89 (2015).